BeBeC-2016-D12

FUNCTIONAL BEAMFORMING APPLIED TO FULL SCALE LANDING AIRCRAFT

Roberto Merino-Martinez[1], Mirjam Snellen[1] and Dick G. Simons[1]
[1]Faculty of Aerospace Engineering, Delft University of Technology
Kluyverweg 1, 2629 HS, Delft, Netherlands

Abstract

Aircraft noise is becoming an increasingly important problem for the aerospace industry and for the residents living in the vicinities of airports. For efforts aiming at reducing aircraft noise levels, it is important to know all the aircraft elements which generate noise and their relative contribution. Experimental measurements with aircraft under operational conditions provide essential information for this purpose. The use of microphone arrays and high resolution beamforming techniques are required to image the acoustic sources at the relatively large distance between the observer and the aircraft. Functional beamforming is a novel nonlinear technique which offers improved array spatial resolution and dynamic range. For an appropriately selected exponent value, most array sidelobes are substantially decreased. This method requires a similar computational time as the conventional beamforming algorithm. In this research, the performance of functional beamforming is investigated with full scale aircraft under operational conditions. The sound of 115 landing aircraft fly-overs was recorded in Amsterdam Airport Schiphol utilizing a 32 microphone array. It was found that functional beamforming provides a good performance, allowing for the identification of individual noise sources on the aircraft. The dynamic range obtained is approximately 30 times larger and its array spatial resolution is about 6 times better than the conventional beamformer.

1 INTRODUCTION

Nowadays, aircraft noise is one of the major problems the aerospace industry has to deal with. Moreover, it is an important cause of annoyance for the population in the surroundings of airports. The continuous increase of air traffic (around a 5% rate per year [1]) and stricter noise regulations are expected to aggravate this issue even more in the future.

During the last decades, significant improvements in the noise levels produced by individual aircraft have been achieved. The largest noise reductions have been experienced by the engine

noise, with technologies such as high bypass ratio turbofan engines and acoustic lining. Therefore, airframe noise (which is produced by the interaction of the aerodynamic surfaces and the surrounding turbulent flow [2]) becomes considerably more important, producing roughly the same Sound Pressure Level (SPL) as the engines in some occasions. This situation is especially noticeable during approach, when the engines operate at low thrust settings and the high lift devices and the landing gear system are extended. It is essential to accurately determine all the noise sources on an aircraft and evaluate their relative contributions to the total noise level, in order to further decrease the noise emissions [3].

Due to their acoustic imaging capabilities, microphone arrays are very useful tools for that purpose. Despite being widely used in the aerospace industry for wind tunnel experiments [4–13], conventional beamforming techniques do not provide sufficient array spatial resolution for full scale aircraft fly-over measurements, due to the typically large distance between the sound source and the observer. Recently, a new beamforming method called functional beamforming was introduced by Dougherty [14, 15]. This method seems to be a promising alternative, providing significantly larger dynamic range and better array spatial resolution than the conventional beamforming technique.

In this research, the noise of 115 fly-overs were recorded using a 32 microphone array at Amsterdam Airport Schiphol. In order to assess its performance, functional beamforming was applied to the acoustic data and compared to other imaging methods such as CLEAN-PSF [16], CLEAN-SC [17] and Robust Adaptive Beamforming (RAB) [18–20]. These results are also presented more extensively.

2 EXPERIMENTAL SET-UP

In this research, a measurement campaign was held at Amsterdam Airport Schiphol utilizing a 32 microphone array in a spiral distribution, see Fig. 1 (a). Previous experiments [21] showed that this array configuration with varying element spacing provides acceptable results over a considerable wide frequency range with a small amount of sidelobes. The array has an effective diameter of 1.7 m and the data is band filtered in the frequency range from 45 Hz to 11,200 Hz. The sampling frequency employed was 40 kHz. In addition, an optical camera is integrated in the centre of the array at a fixed angle facing straight up from the ground.

Aircraft trajectories are considerably less variable during approach than during take-off, since all aircraft follow the Instrument Landing System (ILS) procedure. Moreover, the main reason for only considering landing aircraft in this research is because the engines typically operate at approach idle in this stage. Thus, engine noise is comparably less dominant and other noise sources, such as airframe noise, are more likely to be identified. Therefore, the microphone array was installed 1240 m to the South of the threshold of the Aalsmeerbaan runway (36R), mainly used for landing, see Fig. 1 (b). The measurements took place during two days with similar weather conditions, no precipitations and low wind speeds [22]. In total, 115 aircraft fly-overs were recorded, which correspond to 13 different aircraft families with different turbofan engines.

In addition to the acoustic data, the flight trajectories need to be accurately determined and synchronised with the acoustic data in order to account for propagation, moving source and Doppler effects, as will be described later in subsection 3.1. In order to determine the aircraft positions and velocities, data from three different sources was employed [23]: the ADS-B (Au-

(a) (b)

Figure 1: (a) 32 Microphone array configuration in spiral distribution. (b) Experimental set-up located 1,240 m to the South of the threshold of the Aalsmeerbaan (36R) Schiphol airport runway.

tomatic Dependent Surveillance-Broadcast), the ground radar from Air Traffic Control and the extrapolation of the images from the optical camera. While the three methods provided similar results, the latter one is preferred due to its availability and its ease to combine with the beamforming source plots. The calculated average flight overhead height and aircraft velocity were 67 m and 271 km/h respectively.

3 DATA PROCESSING

3.1 Propagation effects

Prior to the application of any beamforming algorithm, the recorded acoustic data needs to be corrected for several propagation effects. These corrections require as input the aircraft flight trajectories, as mentioned in section 2:

- First, the background noise, such as the ambient noise or the noise generated by the microphone array electronics, should be minimized in order to avoid amplification errors later on. To that end, all the SPL values in the spectrograms under a 30 dB threshold (typical SPL in a quiet library) were neglected.
- Since the aircraft have a relative motion with respect to the observer, the Doppler effect has to be corrected as explained by Howell et al. [24].
- In order to obtain the SPL at the source, the corresponding geometrical spreading from the source location to the observer needs to be added to the recorded SPL.
- Lastly, the consideration of the atmospheric absorption of the sound is also required, which depends on the sound frequency and the atmospheric temperature, static pressure and relative humidity [25, 26].

The result of all the listed corrections is shown in Fig. 2 for two spectrograms of a representative fly-over: the one on the left depicts the signal at the array before any correction and the

one on the right shows the signal at the source after the corrections. Notice the different decibel colour scales and the change in the Doppler shifted tones to straight lines.

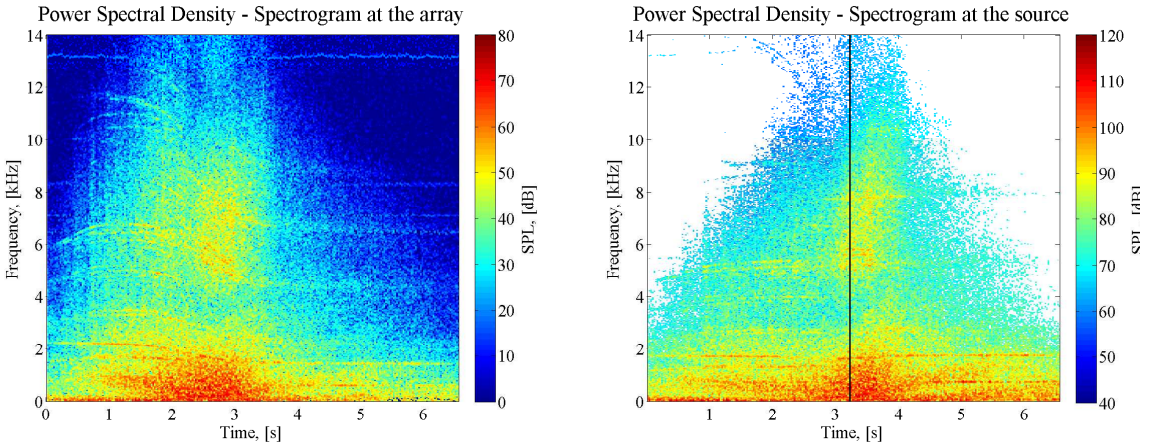

(a) (b)

Figure 2: (a) Spectrogram of the signal recorded at the array during an Airbus A321 fly-over. (b) Spectrogram at the source after applying the mentioned corrections. The solid black line represents the time overhead.

3.2 Functional beamforming

The majority of the beamforming algorithms are based on the phase delays between the emitted sound signal at the source and the received signals at each microphone in the array. The so-called delay-and-sum method or Conventional Frequency Domain Beamformer (CFDBF) [27] is one of the simplest, fastest and most robust algorithms and it is widely used in aeroacoustic experiments, since it allows for a frequency analysis [4–13].

Unfortunately, the CFDBFD offers a dynamic range (or sidelobe level, typically defined as the difference in dB between the main lobe and the highest sidelobe [28]) and an array spatial resolution (i.e. the width of the main lobe 3 dB below its peak [29]) which are not suitable for aircraft fly-over measurements, due to the relative large distance between the sound source (i.e. the aircraft) and the observer. Therefore, it was decided to employ a novel beamforming algorithm called functional beamforming, which was developed by Dougherty in 2014 [14, 15]. This method is based on the CFDBF and the formulae for a general case of a N-microphone array are described below. This method depends on an exponent parameter, ν, selected by the user.

Firstly, the Cross Spectral Matrix ($\mathbf{C}$) is expressed as its eigenvalue decomposition:

$$\mathbf{C} = \frac{1}{2}\mathbf{p}\mathbf{p}^* = \mathbf{U}\mathbf{\Sigma}\mathbf{U}^* \tag{1}$$

where an asterisk, $(\cdot)^*$, denotes the complex conjugate transpose, $\mathbf{p} = \mathbf{p}(f) \in \mathbb{C}^{Nx1}$ is a vector which contains the Fourier transform of the recorded pressure amplitudes for each microphone at a frequency f, $\mathbf{U}$ is a unitary matrix whose columns are the eigenvectors $(\mathbf{u}_1, \ldots, \mathbf{u}_N)$ of $\mathbf{C}$ and $\mathbf{\Sigma}$ is a diagonal matrix whose diagonal elements are the eigenvalues $(\sigma_1, \ldots, \sigma_N)$ of $\mathbf{C}$.

For beamforming, a scan grid is defined which contains all the potential sound source positions. For each grid point position, $\boldsymbol{\xi}_j$, a steering vector, $\mathbf{g}_j \in \mathbb{C}^{Nx1}$, is determined, which accounts for the phase delay and amplitude loss between the sound source and each microphone. Here, j represents the index of the grid point. Each steering vector has N components, $g_{j,n}$, $n = 1 \ldots N$, which are the modeled pressures at each microphone location for a source of unit strength [11] at the considered grid point with position vector $\boldsymbol{\xi}_j$:

$$g_{j,n} = \frac{-\exp(-2\pi i f \Delta t_{j,n})}{4\pi \|\mathbf{x}_n - \boldsymbol{\xi}_j\|(1 - \|\mathbf{M}\|\cos(\theta))^2} \tag{2}$$

where $\|\cdot\|$ is the Euclidean norm of the vector, $i = \sqrt{-1}$, $\Delta t_{j,n}$ is the time delay between the emission at the source and the reception of the signal by the observer, $\mathbf{x}_n = (x_n, y_n, z_n \in \mathbb{R}^{Nx1})$, $n = 1 \ldots N$, are the position vectors of the N microphones, $\mathbf{M}$ is the Mach number vector, $\mathbf{M} = \mathbf{V}/c$, $\mathbf{V}$ is the source velocity vector, c is the sound speed and θ is the angle between the relative position vector of the source with respect to the observer and the source velocity vector, $\mathbf{V}$. In case of a moving source, such as an aircraft flying by, $\mathbf{M} \neq \mathbf{0}$ and the term between parenthesis in the denominator in Eq. 2 represents the so-called convective amplification. The moving source effect also needs to be taken into account [23, 28] when calculating the time delays, $\Delta t_{j,n}$.

The general formula for the functional beamformer for a grid point located at $\boldsymbol{\xi}_j$ and an exponent value of ν is:

$$A_\nu(\boldsymbol{\xi}_j) = [\mathbf{w}_j^* \mathbf{C}^{\frac{1}{\nu}} \mathbf{w}_j]^\nu = [\mathbf{w}_j^* \mathbf{U} \boldsymbol{\Sigma}^{\frac{1}{\nu}} \mathbf{U}^* \mathbf{w}_j]^\nu \tag{3}$$

where A_ν is the estimate for the source autopower at grid point $\boldsymbol{\xi}_j$ for an exponent ν. Notice that the case with $\nu = 1$ corresponds to the CFDBF formula. In Eq. 3, $\mathbf{w}_j \in \mathbb{C}^{Nx1}$ is the normalized steering vector (also known as weight vector [17]), $\mathbf{g}_j$, for that grid point $\boldsymbol{\xi}_j$. There are several possible definitions for the weight vector in literature [30], with a compromise solution in both determining the exact source location and the correct source strength. For this research, since all the acoustic sources considered are close to the nadir direction of the array, the following formulation was selected, which provides the correct source strength with negligible deviations in the source position:

$$\mathbf{w}_j = \frac{\mathbf{g}_j}{\|\mathbf{g}_j\|^2} \tag{4}$$

The performance of functional beamforming is determined by the exponent parameter ν. This can be observed when considering an example with a single point sound source of amplitude s_k with position vector $\boldsymbol{\xi}_k$. In that case, the dominant eigenvalue of $\mathbf{C}$ will be $\sigma_1 = s_k^2/2$ with the corresponding eigenvector $\mathbf{u}_1 = \mathbf{g}_k$. Introducing Eq. 4 in Eq. 3, the functional beamforming autopower value for a general location $\boldsymbol{\xi}_m$ with steering vector $\mathbf{g}_m$, i.e. the Point Spread Function (PSF) [29], will now be:

$$A_\nu(\boldsymbol{\xi}_m) = \left[\mathbf{w}_m^* \mathbf{C}^{\frac{1}{\nu}} \mathbf{w}_m\right]^\nu = \left[\frac{\mathbf{g}_m^* \left(\frac{1}{2} s_k^2 \mathbf{g}_k \mathbf{g}_k^*\right)^{\frac{1}{\nu}} \mathbf{g}_m}{\|\mathbf{g}_m\|^4}\right]^\nu = \frac{1}{2} s_k^2 \left[\frac{\mathbf{g}_m^* \mathbf{g}_k \mathbf{g}_k^* \mathbf{g}_m}{\|\mathbf{g}_m\|^4}\right]^\nu = \frac{1}{2} s_k^2 \left[\frac{\left(\mathbf{g}_m^* \mathbf{g}_k\right)^2}{\|\mathbf{g}_m\|^4}\right]^\nu \tag{5}$$

where it was used that $\mathbf{g}_k \mathbf{g}_k^*$ is an idempotent matrix i.e. $(\mathbf{g}_k \mathbf{g}_k^*)^x = \mathbf{g}_k \mathbf{g}_k^*, \forall x \in \mathbb{R}$. It can be

observed that the PSF factor multiplying the source strength is powered to the exponent ν. This factor has a value of 1 at the correct source locations and alias point (i.e. the so-called grading lobes) and smaller than 1 everywhere else. Hence, powering this factor at a sidelobe location to an exponent larger than 1 will lower its level, keeping the values for the true sources identical, if a suitable grid is used. For ideal conditions, the dynamic range (in dB) for the functional beamforming increases linearly with the value of the exponent, ν. Thus, for an appropriate exponent value, the dynamic range is considerably increased. Previous experience [23] showed that for a value of $\nu = 100$ acceptable results are obtained. The main lobes are also sharpened, improving the array spatial resolution to some extent. The detection of two sources closely spaced is still limited by the Rayleigh criterion [23, 31]. Moreover, the computational demand for the functional beamforming is practically identical to the CFDBF case, since the only relevant additional operation is the eigenvalue decomposition of the matrix $\mathbf{C}$, which is typically faster than the rest of steps involved in the beamforming process.

One of the main advantages of the functional beamforming technique is that it preserves noise sources with lower amplitude than the strongest source. This can be observed in Fig. 3, which shows the results for a simulation with three different point sources: one 100 dB source at (0, 0) m, one 90 dB source at (0.875, 0.290) m and one 80 dB source at (0.7, -0.5) m, all emitting sound at 3 kHz and located 1 m away from the microphone array. The array considered in this simulation has the same microphone distribution as the used in the experimental set-up, see Fig. 1 (a). It can be seen that the weaker sources cannot be properly identified in the CFDBF case, due to the abundance of high sidelobes of approximately the same SPL, while functional beamforming succeeds in clearly separating all sources at the correct source locations and with the correct strengths.

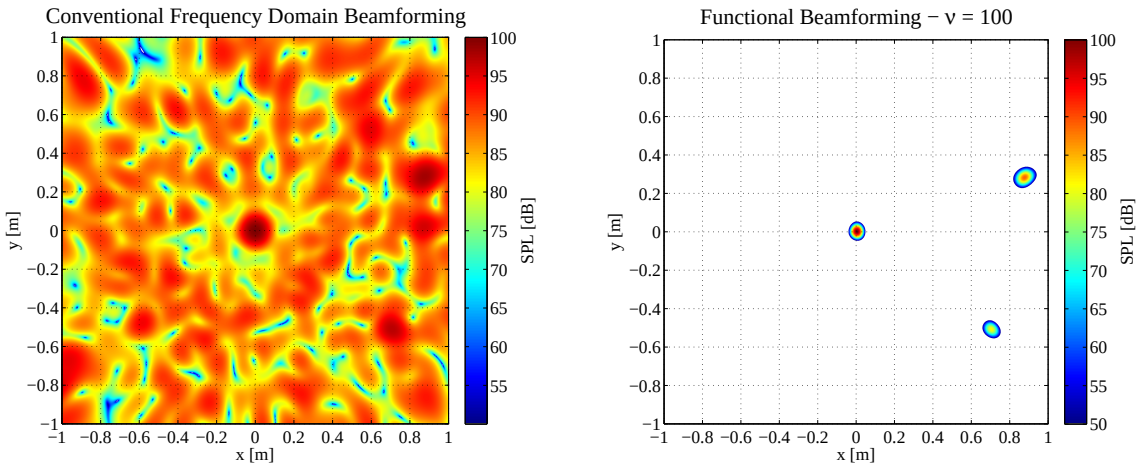

Figure 3: Comparison between the results of (a) CFDBF ($\nu = 1$) and (b) functional beamforming with $\nu = 100$ for three simulated sources: one 100 dB source at (0, 0) m, one 90 dB source at (0.875, 0.290) m and one 80 dB souce at (0.7, -0.5) m, all emitting at 3 kHz and situated 1 m away from the array.

This algorithm has been tested in numerical simulations [14, 15, 23] and idealized experimental cases with speakers as sound sources and experiments in controlled conditions in a

laboratory [14, 15]. This method was applied for the first time to full scale aircraft during operational conditions by the authors [23]. The present paper gathers the most relevant results.

4 EXPERIMENTAL RESULTS

4.1 Comparison of functional beamforming with other imaging methods

In order to assess the performance of the functional beamforming algorithm with experimental data, the 115 recorded fly-over measurements were used. Out of the 115 results, two representative examples are presented, which correspond to two different aircraft types (Airbus A321 and Fokker 70), which typically present strong airframe noise sources during landing [32]. In particular, beamforming was applied to one specific frequency in each case: 1629 Hz for the Airbus A321 and 7138 Hz for the Fokker 70. These frequencies were selected after observing that they were clear peaks in the frequency spectra for each case at the overhead time, as shown in Fig. 4. Moreover, the results obtained using functional beamforming are compared to the ones using other methods, such as: CFDBF[27], CLEAN-PSF [16], CLEAN-SC [17] and Robust Adaptive Beamforming (RAB) [18–20].

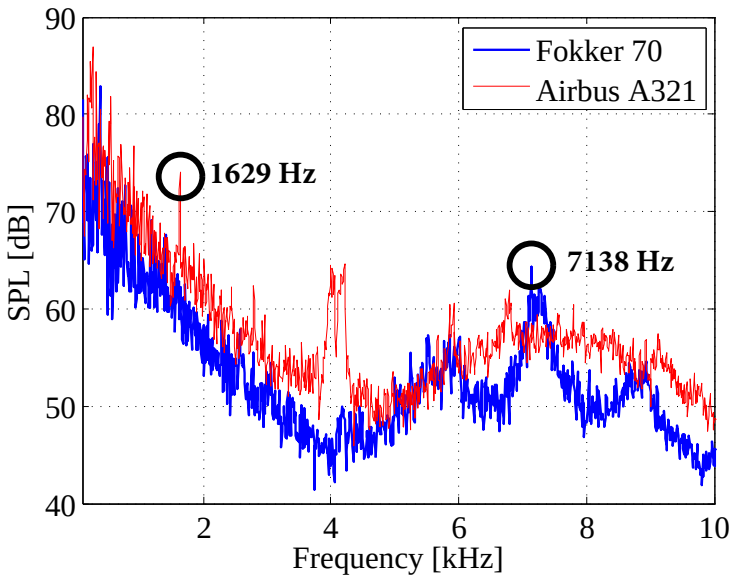

Figure 4: Sound frequency spectra during the time overhead (using a 0.1 s time window) for a fly-over measurement of an Airbus A321 (red) and a Fokker 70 (blue).

The results of all methods for the Airbus A321 fly-over are depicted in Fig. 5 . A 60 dB range was selected in the source maps in order to show possible sidelobes. The aircraft outline has been manually added to the plots for clarity reasons. After beamforming, it was determined that the dominant noise source at 1629 Hz is the nose landing gear. The CFDBF source plot presents a very wide lobe pointing approximately to the nose landing gear location, but it is heavily contaminated with sidelobes, hindering the identification of noise sources. Using functional beamforming with an exponent value of $\nu = 100$ makes the sidelobes virtually disappear and the array spatial resolution is approximately 6 times narrower [23]. The CLEAN-PSF technique

enhances to some extent the CFDBF results, identifying the source location, but the source map still presents several sidelobes of lower level, which can be confused with real sources. The CLEAN-SC algorithm overcomes this issue, providing the correct source location with virtually no sidelobes. The array spatial resolution in both CLEAN cases is selected by the user. In the figures presented here, the beamwidth of the main lobe was plotted large enough for clarity reasons. Finally, the RAB method was used with a diagonal loading parameter, μ, value of 0.005, which was determined iteratively. Due to its sensitivity to perturbations and experimental errors, this method provides results of lower quality compared to the ones with simulated data [23], but still improves the source plot of the CFDBF.

The dynamic range obtained by each method for the A321 fly-over data was calculated and depicted in Fig. 5 (f), as well as the corresponding dynamic range achieved using simulated data of a point sound source at the same position and of the same strength and frequency as the one considered here [23]. Most algorithms have a comparable dynamic range in both cases, except the RAB method, which experiences a reduction of more than 70% of its dynamic range for the experimental case compared to the synthetic case. It can be noticed that the functional beamforming and CLEAN-SC methods provide the best results in both cases.

For the Fokker 70 fly-over, a 12 dB range was chosen for presenting the beamforming source maps of Fig. 6, because higher frequencies typically present more sidelobes and of higher level. Looking at the beamforming source plots, it seems that the dominant noise source at 7138 Hz is the main landing gear system. However, the CFDBF also presents several sidelobes that could be mistaken for actual sources. Functional beamforming solves this problem, eliminating again all the sidelobes for this dB range. The CLEAN-PSF method identifies both sound sources from the main landing gear, but the source map still presents many strong sidelobes. It is interesting to notice that the CLEAN-SC algorithm is unable to identify both sources, detecting only the strongest one. This is the main disadvantage of this method, since it cannot detect two or more sound sources emitting at the same frequency. The RAB technique required a diagonal loading parameter of $\mu = 0.1$, which is 100 times larger than for the low frequency case of the A321, due to the higher frequency considered [18–20]. Once again, this method improves the CFDBF results to some extent, but still presents significant sidelobes.

The dynamic ranges provided by all methods with the Fokker 70 measurement are gathered in Fig. 6 (f), as well as the corresponding dynamic range obtained using simulated data of two point sound sources at the same positions and of the same strength and frequency as the ones considered here [23]. Most algorithms offer similar values in both cases, which are comparably lower than for the lower frequency case studied in Fig. 5, except the CLEAN-SC method, which presents the same dynamic range for all cases.

4.2 Array spatial resolution improvement

The variation of the array spatial resolution (relative to the CFDBF value) with the functional beamforming exponent, ν, is presented in Fig. 7. The same microphone array distribution as in Fig. 1 (a) was used. The exponents range from 1 to 500. In the plot the obtained beamwidths 3 dB below the peak for both the experimental data of the Airbus A321 source at 1629 Hz and simulations with a point source with the same conditions [23] are included. The behaviors in both cases are in good agreement. It can be observed that the relative beamwidth rapidly decreases with increasing ν.

However, after a threshold value of around 100, it remains approximately constant. This

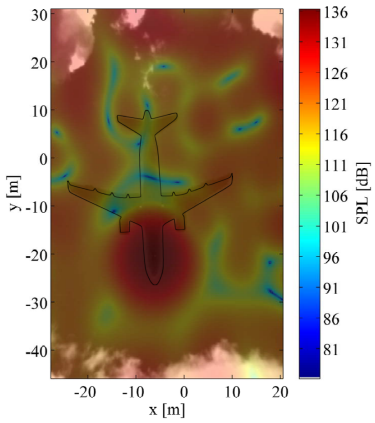

(a) CFDBF

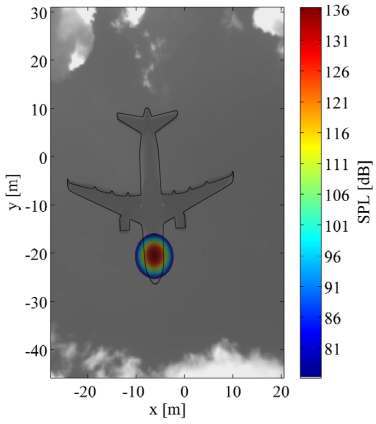

(b) Functional ($\nu = 100$)

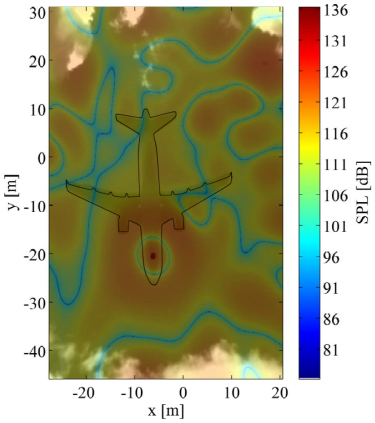

(c) CLEAN-PSF

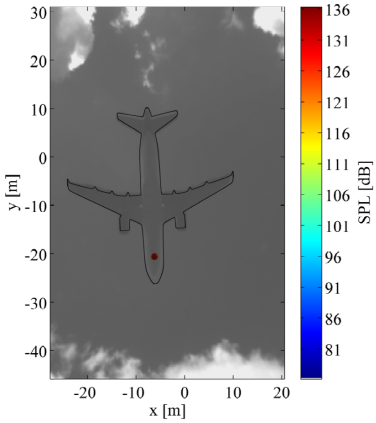

(d) CLEAN-SC

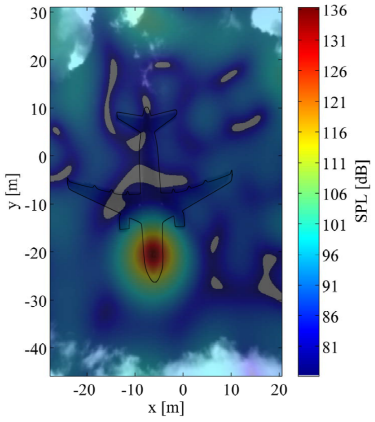

(e) RAB ($\mu = 0.005$)

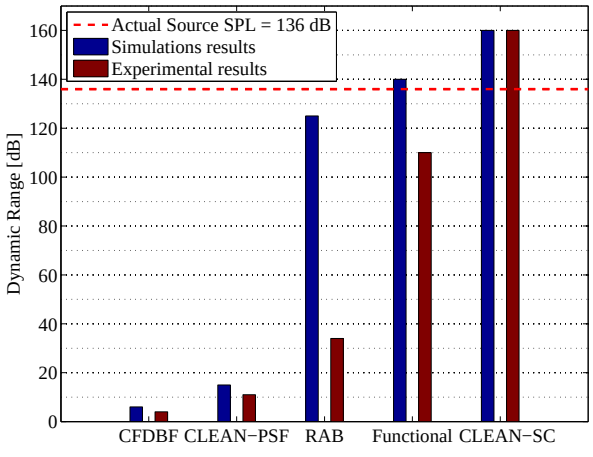

(f)

Figure 5: Comparison between the beamforming source plots for an Airbus A321 fly-over at 1629 Hz using different algorithms: (a) CFDBF. (b) Functional beamforming ($\nu = 100$). (c) CLEAN-PSF. (d) CLEAN-SC and (e) RAB ($\mu = 0.005$). (f) Comparison between the dynamic range obtained for the simulated and experimental data. Reproduced from [23].

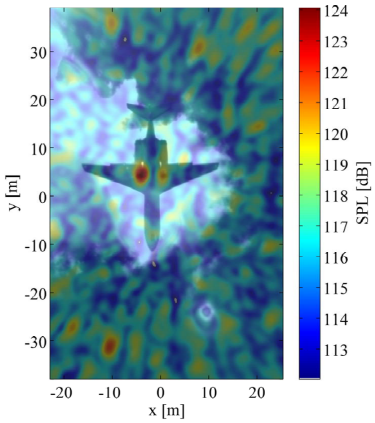

(a) CFDBF

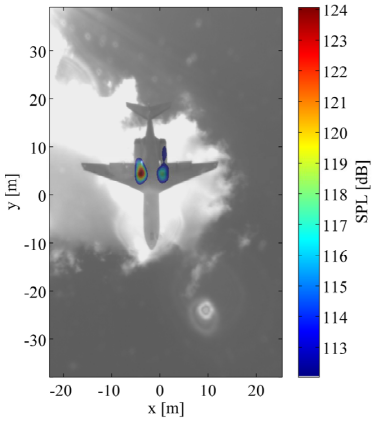

(b) Functional ($\nu = 100$)

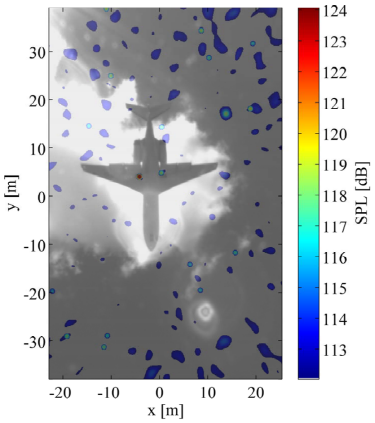

(c) CLEAN-PSF

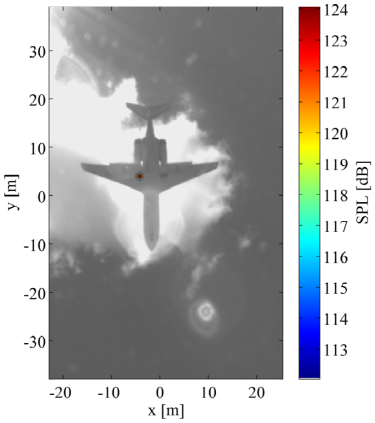

(d) CLEAN-SC

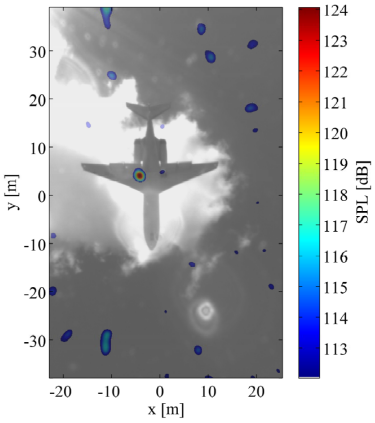

(e) RAB ($\mu = 0.1$)

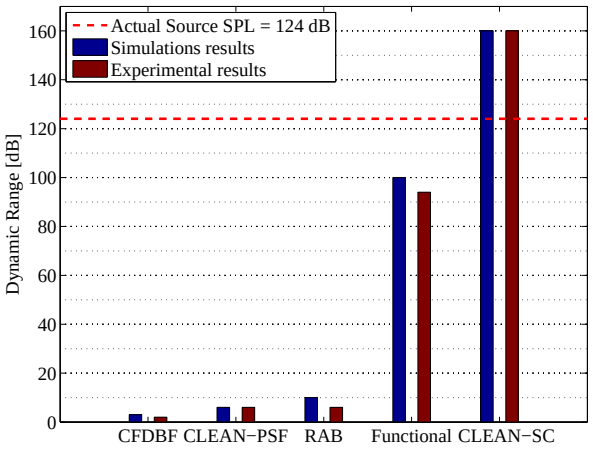

(f)

Figure 6: Comparison between the beamforming source plots for a Fokker 70 fly-over at 7138 Hz using different algorithms: (a) CFDBF. (b) Functional beamforming ($\nu = 100$). (c) CLEAN-PSF. (d) CLEAN-SC and (e) RAB ($\mu = 0.1$). (f) Comparison between the dynamic range obtained for the simulated and experimental data. Reproduced from [23].

explains why a value of $\nu = 100$ was chosen for this study. The beamwidth for that exponent value is approximately 6 times narrower than for the CFDBF case.

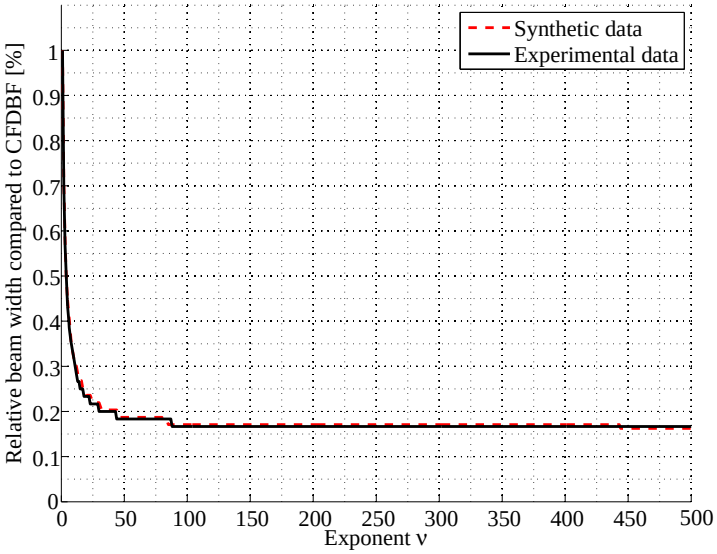

Figure 7: Array spatial resolution for functional beamforming as a function of the exponent ν compared to the ones obtained with the CFDBF algorithm ($\nu = 1$) for simulated and experimental data for a single 1629 Hz sound source case.

5 CONCLUSIONS

A novel beamforming algorithm called functional beamforming is applied to the noise of full scale aircraft during operational conditions. The performance of this method was assessed and compared to other acoustic imaging techniques, such as CFDBF, CLEAN-PSF, CLEAN-SC and RAB.

Functional beamforming is a promising alternative for the CFDBF method as the standard beamforming algorithm used for aeroacoustic experiments, since it provides a dynamic range around 30 to 40 times larger and an array spatial resolution approximately 6 times better than the CFDBF, requiring a similar computational time. The only method analyzed in this paper that is also capable of clearly identifying the strongest sound source is the CLEAN-SC. However, the CLEAN-SC is unable to identify multiple sources emitting sound at the same frequency, unlike the functional beamforming method.

This paper studies airframe noise sources, particularly landing gear noise, which are dominant for certain aircraft types during landing. These sound sources might be overlooked by the CFDBF method, but are clearly detected by the functional beamforming technique.

References

[1] "Current market outlook 2013-2032," tech. rep., Boeing Commercial Airplanes, USA., 2013.

[2] M. J. Lighthill, "On sound generated aerodynamically, I: General theory.," *Proceedings of the Royal Society of London. Series A, Mathematical and Physical Sciences.*, vol. 221, pp. 564–587, 1952.

[3] D. G. Simons, M. Snellen, B. Midden, M. Arntzen, and D. H. T. Bergmans, "Assessment of noise level variations of aircraft fly-overs using acoustic arrays," *Journal of Aircraft*, vol. 52, pp. 1625–1633, September-October 2015.

[4] Y. Liu, A. R. Quayle, A. P. Dowling, and P. Sijtsma, "Beamforming correction for dipole measurement using two-dimensional microphone arrays," *J. Acoust. Soc. Am.*, vol. 124, pp. 182–191, July 2008.

[5] C. Camier, T. Padois, J. Provencher, P. Gauthier, A. Berry, J. Blais, M. Patenaude-Dufour, and R. Lapointe, "Fly-over source localization on civil aircraft," in *Proceedings of the* 19th *AIAA/CEAS Aeroacoustics Conference. 27-29 May 2013. Berlin, Germany*, 2013. AIAA paper 2013-2261.

[6] R. P. Dougherty, R. C. Ramachandran, and G. Raman, "Deconvolution of sources in aeroacoustic images from phased microphone arrays using linear programming," in *Proceedings of the* 19^{t}*h AIAA/CEAS Aeroacoustics Conference, Berlin, Germany, 27th-29th May 2013*, May 2013. AIAA paper 2013-2210.

[7] Y. Ishii, J. Hald, T. Ishii, H. Oinuma, K. Nagai, Y. Yokokawa, and K. Yamamoto, "High-resolution fly-over beamforming using a practical array," in *Proceedings on CD of the* 5th *Berlin Beamforming Conference, 19-20 February 2014*, GFaI, e.V., Berlin, February 2014.

[8] U. Michel, B. Barsikow, J. Helbig, M. Hellmig, and M. Schüttpelz, "Flyover noise measurements on landing aircraft with a microphone array," in *Proceedings of the* 4th *AIAA/CEAS Aeroacoustics Conference, Toulouse, France, June 2-4, 1998*, June 1998. AIAA paper 1998-2336.

[9] G. Herold and E. Sarradj, "Preliminary benchmarking of microphone array methods," in *Proceedings on CD of the 5th Berlin Beamforming Conference, 19-20 February 2014*, GFaI, e.V., Berlin, February 2014.

[10] H. Siller, "Localisation of sound sources on aircraft in flight," in *Proceedings on CD of the* 4th *Berlin Beamforming Conference, 22-23 February 2012*, GFaI, e.V., Berlin, February 2012.

[11] P. Sijtsma, "Phased array beamforming applied to wind tunnel and fly-over tests," Tech. Rep. NLR-TP-2010-549, National Aerospace Laboratory (NLR), December 2010.

[12] P. Sijtsma and R. Stoker, "Determination of Absolute Contributions of Aircraft Noise Components Using Fly-over Array Measurements," in *Proceedings of the* 10^{th} *AIAA/CEAS Aeroacoustics Conference, Manchester, United Kingdom, 10-12 May 2004*, 2004. AIAA paper 2004-2958.

[13] T. Sinnige, A. M. N. Malgoezar, D. Ragni, K. Y. W. Scheper, M. Snellen, G. Eitelberg, and L. L. M. Veldhuis, "Apian-inf: a low-speed aerodynamic and aeroacoustic investigation of pylon-pusher propeller interaction effects," in *Proceedings of the* 5^{th} *CEAS Air & Space Conference. Challenges in European Aerospace. Delft, Netherlands. 7-11 September 2015*, 2015.

[14] R. P. Dougherty, "Functional beamforming," in *Proceedings on CD of the* 5^{th} *Berlin Beamforming Conference, 19-20 February 2014. Berlin, Germany.*, GFaI, e.V., Berlin, February 2014.

[15] R. P. Dougherty, "Functional beamforming for aeroacoustic source distributions," in *Proceedings of the* 20^{th} *AIAA/CEAS Aeroacoustics Conference. 16-20 June 2014. Atlanta GA, USA.*, 2014. AIAA paper 2014-3066.

[16] J. A. Hogbom, "Aperture synthesis with a non-regular distribution of interferometer baselines," *Astron. Astrophys. Suppl.*, vol. 15, pp. 417–426, 1974.

[17] P. Sijtsma, "CLEAN based on spatial source coherence," *International Journal of Aeroacoustics*, vol. 6, pp. 357–374, 2007.

[18] J. Li, P. Stoica, and W. Wang, "On robust capon beamforming and diagonal loading," *IEEE Transactions on Acoustics Speech and Signal Processing*, vol. 51, pp. 1702–1715, July 2003.

[19] H. Cox, R. Zeskind, and M. Owen, "Robust adaptive beamforming," *IEEE Transactions on Acoustics Speech and Signal Processing*, vol. ASSP-35, pp. 1365–1367, October 1987.

[20] X. Huang, L. Bai, I. Vinogradov, and E. Peers, "Adaptive beamforming for array signal processing in aeroacoustic measurements," *Journal of the Acoustical Society of America*, pp. 2152–2161, March 2012.

[21] R. van der Goot, J. Hendriks, S. K. Y. W., W. Hermans, G.and van der Wal, and D. G. Simons, "A low cost, high resolution acoustic camera with a flexible microphone configuration," in *Proceedings on CD of the 4th Berlin Beamforming Conference, 22-23 February 2012*, GFaI, e.V., Berlin, February 2012.

[22] M. Snellen, R. Merino-Martinez, and D. G. Simons, "Assessment of aircraft noise sources variability using an acoustic camera," in *Proceedings of the* 5^{th} *CEAS Air & Space Conference. Challenges in European Aerospace. Delft, Netherlands. 7-11 September 2015*, 2015.

[23] R. Merino-Martinez, M. Snellen, and D. G. Simons, "Functional beamforming applied to imaging of fly-over noise on landing aircraft," *Journal of Aircraft*, 2016. Paper accepted for publication.

[24] G. P. Howell, M. A. Bradley, M. A. McCormick, and J. D. Brown, "De-Dopplerization and acoustic imaging of aircraft Flyover noise measurements," *J. Sound Vib.*, vol. 105, pp. 151–167, Feb 1986.

[25] M. Arntzen, *Aircraft noise calculation and synthesis in a non-standard atmosphere*. PhD thesis, Delft University of Technology (PhD thesis), 2014.

[26] G. Ruijgrok, *Elements of aviation acoustics*. VSSD, Second ed., 2007. ISBN-1090-6562-155-5.

[27] D. H. Johnson and D. E. Dudgeon, *Array Signal Processing, Concepts and Techniques*. P T R Prentice Hall, Englewood Cliffs, 1993.

[28] P. Sijtsma, "Experimental techniques for identification and characterisation of noise sources," Tech. Rep. NLR-TP-2004-165, National Aerospace Laboratory (NLR), April 2004.

[29] T. Mueller, *Aeroacoustic Measurements*. Springer, First ed., 2002. ISBN-978-3-642-07514-8.

[30] E. Sarradj, "Three-dimensional acoustic source mapping with different beamforming steering vector formulations," *Advances in Acoustics and Vibration*, vol. 2012, no. 292695, pp. 1–12, 2012.

[31] F. R. S. Lord Rayleigh, "Xxxi. investigations in optics with special reference to the spectroscope," *The London, Edinburgh and Dublin Philosophical Magazine and Journal of Science*, vol. Fifth Series, pp. 261–274, October 1879.

[32] M. Snellen, R. Merino-Martinez, and D. G. Simons, "Assessment of noise level variability on landing aircraft using a microphone array," *Journal of Aircraft*, no. Paper submitted for publication., 2016.